Chemosphere 335 (2023) 139173

Contents lists available at ScienceDirect

Chemosphere

journal homepage: www.elsevier.com/locate/chemosphere

Novel Sb-doped SnO_2 ceramic anode coated with a photoactive $BiPO_4$ layer for the photoelectrochemical degradation of an emerging pollutant

A. Balseviciute [a], M.C. Martí-Calatayud [a], V. Pérez-Herranz [a], S. Mestre [b], M. García-Gabaldón [a,*]

[a] IEC Group, Instituto de Seguridad Industrial, Radiofísica y Medioambiental, Universitat Politècnica de València, Camí de Vera, S/n, 46022, València, Spain
[b] University Institute of Ceramic Technology, Chemical Engineering Department, Universitat Jaume I, Castellón, Spain

HIGHLIGHTS

- A Sb-doped SnO2 anode with a photocatalytic layer of BiPO4 was studied.
- The material has enhanced photoactivity at potential values of around 2.5 V.
- The anode exhibited lower charge-transfer in the presence of light.
- Higher mineralization degree of NOR was obtained for larger illuminated areas.
- The decomposition of NOR followed mixed-order kinetics.

GRAPHICAL ABSTRACT

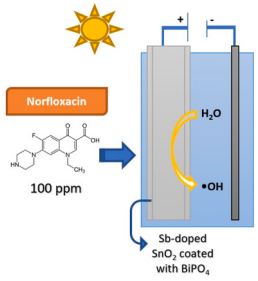

ARTICLE INFO

Handling Editor: E. Brillas

Keywords:
Norfloxacin
Mineralization
Photocatalyst
BiPO4 layer
Sb–SnO_2 ceramic electrode
Advanced oxidation processes

ABSTRACT

In the present work, a study about the electrochemical and photoelectrochemical degradation of an emerging pollutant using an Sb-doped SnO_2 anode coated with a photocatalytic layer of $BiPO_4$ has been performed. The electrochemical characterization of the material was carried out by means of linear sweep voltammetry, light-pulsed chronoamperometry and electrochemical impedance spectroscopy. These studies confirmed that the material is photoactive at intermediate potential values (around 2.5 V), and that the charge transfer resistance decreases in the presence of light.

A positive effect of the illuminated area on the degradation degree of norfloxacin was observed: at 15.50 mA cm^{-2}, the degradation rate was 83.37% in the absence of light, 92.24% with an illuminated area of 5.7 cm^2, and it increased up to 98.82% with an illuminated area of 11.4 cm^2. The kinetics of the process were evaluated, and the by-products of the degradation were identified by ion chromatography and HPLC. In the case of the mineralization degree, the effect of light is less significant, especially at higher current densities. The specific energy consumption of the process was lower in the photoelectrochemical experiments as compared to the experiments in dark conditions. At intermediate current densities (15.50 mA cm^{-2}) a decrease in energy consumption of 53% was achieved by illuminating the electrode.

* Corresponding author.
E-mail address: mongarga@iqn.upv.es (M. García-Gabaldón).

https://doi.org/10.1016/j.chemosphere.2023.139173
Received 11 April 2023; Received in revised form 6 June 2023; Accepted 7 June 2023
Available online 8 June 2023

1. Introduction

Today, one of the most concerning environmental problems is the excessive and poorly controlled use of pharmaceuticals, personal care products and fertilizers, among others. Part of these compounds ends up dispersed in the environment (mostly in water and soil) as a consequence of their release from production processes and their overconsumption. They appear in low concentrations, but their effects on the environment and health are still not properly known. UNESCO gives the name of pollutants of emerging concern to these types of compounds, which are mainly high molecular weight organic molecules (UNESCO, 2014).

Antibiotics are a group of such compounds which are highly produced and consumed. Antibiotic consumption was 42.3 billion DDD (Defined Daily Doses) in 2015. With the current consumption trend, an increase of 15% was projected for the period between 2015 and 2030 (Klein et al., 2018). Uncontrolled antibiotic consumption poses a huge risk to the environment because they can return to humans and animals through the trophic chain (Polianciuc et al., 2020). Also, the presence of antibiotics in the environment can lead to the emergence of antibiotic-resistant bacteria (Szymańska et al., 2019).

Wastewater treatment plants with conventional treatments (primary and biological treatments) remove part of the antibiotics, mostly by adsorption, but a variety of highly refractory contaminants is still found in the effluent. Thus, new processes that can completely remove these types of pollutants are needed. Advanced Oxidation Processes (AOPs) have shown high efficiency in terms of removing organic and refractory pollutants (O'Shea and Dionysiou, 2012; Rayaroth et al., 2016; Wang and Zhuan, 2020). The elimination mechanism of these contaminants in AOPs is based on successive oxidation reactions initiated by the generation of oxidizing species. Highly known AOPs are Fenton, ozonation, electrochemical oxidation and photocatalysis (Salimi et al., 2017).

Photocatalysis is a technology that uses the energy of a photon to lower the activation energy of a chemical reaction. Most of the frequently employed photocatalysts are semiconductors. When a semiconductor absorbs light with a higher energy than the band-gap, the electron jumps from the valence to the conduction band, forming an electron/hole pair which reacts with water forming the hydroxyl radical. However, photocatalysts used in wastewater treatment processes also present several disadvantages that hinder their applicability, e.g.:

- Most photocatalysts are used as suspensions in wastewaters which makes difficult their applicability and recoverability.
- Some photocatalysts, such as TiO2 (El Rouby et al., 2019; Peleyeju et al., 2017; Shokri et al., 2016) are only active in the UV light spectrum.
- They have low photoconversion rates because the generated electron/hole pairs recombine quickly (Qian et al., 2019; Seo and Oh, 2019).

One of the proposed solutions to increase the efficiency of the photoconversion process and facilitate the recovery and reuse of photocatalysts is their deposition over a conductive support (Fernández-Ibáñez et al., 2021). Photocatalysts supported on a conductive substrate have been proven to have almost the same efficiency as the suspended ones (Tan and Vinh, 2020). In addition, photocatalysts on a fixed surface do not need to be recovered, which makes possible treating larger amounts of wastewater. In this case, the photochemical •OH generation is combined with the electrochemical one in a process known as photo-electrocatalysis.

In the present work, Sb-doped SnO_2 ceramic electrodes will be used as a support for a bismuth phosphate ($BiPO_4$) photoactive layer. The Sb-doped SnO_2 electrodes were tested in previous works and showed good electrochemical performance as anodes for the degradation of organic compounds because of their porosity and high conductivity (Arenhart Heberle et al., 2019; Droguett et al., 2020; Mora-Gómez et al., 2020). Moreover, they can be synthesized at low production costs, since they are made of cheap materials and using traditional techniques of the ceramic industry. This material displayed a performance in terms of degrading emerging pollutants similar to that obtained with BDD commercial electrodes (Mora-Gómez et al., 2019). Moreover, $BiPO_4$ exhibits high activity as photocatalyst in the visible light spectrum (Li et al., 2011), it is a non-toxic material (Kumar et al., 2022) and has been extensively used in the photocatalytic removal of dyes (Bouddouch et al., 2022; Pan and Zhu, 2010).

The purpose of this investigation is to study the performance of Sb-doped SnO_2 anodes with a photocatalytic layer of $BiPO_4$ in the electrochemical and photoelectrochemical degradation of an emerging pollutant. As a difference to other works in literature, an exhaustive electrochemical characterization of the material has been performed to confirm its photoactivity and select the optimal conditions for the removal of the contaminant. The electrochemical characterization of the anode has been carried out in dark conditions and under the irradiation with a visible light source. Once characterized, the anode has been applied to the photoelectrochemical oxidation of norfloxacin, which has been used as a model emerging pollutant. Norfloxacin is a synthetic broad-spread antibiotic from a group of pharmaceuticals known as fluoroquinolones (Goldstein, 1987). The anode efficiency in the process has been determined by obtaining the degradation and mineralization degrees as well as the energy consumption. The kinetics of the degradation have also been described and evaluated by calculating the kinetic constants of the process.

2. Materials and methods

2.1. Reagents

Tin dioxide (SnO_2) (99.85%, Quimialmel) and antimony dioxide (Sb_2O_3) (99%, Alfa-Aesar) were used for the synthesis of the ceramic electrode along with polyvinyl alcohol (PVA, Mowiol 8–88, Clariant Iberica) as a ligand. The photoactive layer was made using bismuth oxide (Bi_2O_3) (99.99%, Quimialmel), ammonium dihydrogenphosphate, (NH_4)H_2PO_4 (99%, Panreac) and isopropyl myristate (Quimidroga S.A. Spain). Analytical grade sodium sulfate (99%, Panreac) was used as supporting electrolyte in the electrode characterization and in the photoelectrochemical degradation of norfloxacin experiments.

Analytical grade norfloxacin (≥98%, Sigma-Aldrich) was used as a model emerging pollutant, as mentioned above. The determination of total organic carbon (TOC) was performed in acidic media using a 1 M solution of sulfuric acid (98%, J.T. Baker). All solutions were prepared using Type 1 Mili-Q ultrapure water.

Sodium hydrogen carbonate (>99%) and anhydrous sodium carbonate (>99%) (Sigma-Aldrich) were used as phases in the ion chromatography measurements. Analytical grade acetonitrile (Merck), acetic acid (Fischer) and ultrapure type 1 water were used for the HPLC analysis.

Sodium tiosulfate (99%, Sigma-Aldrich), potassium iodide (99%, Honeywell) and a starch solution 1% v/v (Panreac) were used in the iodometric determination of persulfate.

2.2. Physical characterization of the anode

The ceramic substrate was synthesized as described in a previous study (Mora-Gómez et al., 2018). SnO_2, Sb_2O_3 (99/1 M ratio), and the ligand (0.8% in weight) were mixed in a planetary mill at 230 rpm for 1 h. Once mixed, the resulting suspension was thermally treated in an oven at 110 °C for 24 h. The powder was then sieved and humidified at 0.05 kg water/kg dry solid. A uniaxial manual press working at 250 kg cm^{-2} shaped the suspension to its final prismatic form. The size of the synthesized ceramic anode was 80 × 20 × 4 mm.

For the bismuth phosphate layer deposition, ammonium

dihydrogenphosphate and bismuth oxide were dry mixed in a mortar and thermally treated in an electric furnace (RHF1400, Carbolite Furnaces, Lt). The thermal cycle was heating at 10 °C min^{-1} from room temperature up to 700 °C, a soaking time of 4 h and subsequent natural cooling. The product was grinded in an agate mortar and sieved in a 200 μm mesh.

The catalyst suspension was prepared by milling a mixture of powdered $BiPO_4$ and isopropyl myristate with some additives in a planetary mill with microballs (Pulverisette 5, Fritsch GmbH, Germany) for 60 min at 260 rpm. The deposition of the catalyst by dip-coating was carried out in a homemade apparatus, which enables the control of immersion and emersion speeds. After the deposition, the electrodes were dried in an oven and the catalyst was thermally fixed with a treatment based on heating at 10 °C min^{-1} up to 800 °C and 1 h of soaking time in the electric furnace.

The bulk density of ceramic electrodes was measured by mercury immersion (Archimedes' method). The electrical resistivity of the sintered samples was measured by a four-point method with a HIOKI RM3545 equipment (Hioki E.E. Corporation, Japan) and a homemade setup.

Characterization of crystalline structures was performed using an X-ray diffractometer (Theta-Theta D8 Advance, Bruker, Germany), with CuK radiation ($\lambda = 1.54183$ Å). The generator applied a light source of 45 kV and 40 mA. XRD data were collected using of a VÅNTEC-1 detector in a 2θ from 5 to 90° with a step width of 0.015° and a counting time of 1.2 s/step. Images of the electrode surface were taken with a FEG-SEM (QUANTA 200F, FEI Co, USA) coupled with an energy-dispersive X-Ray microanalysis instrument (EDX, Genesis 7000 SUTW; EDAX, Mahwah, NJ) to analyze the characteristics and the composition of the catalyst particles.

2.3. Photoelectrochemical characterization of the anode

The electrochemical characterization of the electrode was carried out by means of linear sweep voltammetry (LSV), pulsed light chronoamperometry, and electrochemical impedance spectroscopy (EIS) using a potentiostat/galvanostat Autolab PGSTAT302 N (Metrohm) and the NOVA 1.10 software.

A conventional 3-electrode cell was used in all electrochemical tests. A Pt-foil (Metrohm) and an Ag/AgCl electrode (3 M KCl) (Crison) were used as counter and reference electrodes, respectively. The working electrode was the Sb-doped SnO_2 anode coated with $BiPO_4$ with an effective area of 0.25 cm^2. The electrochemical tests were performed in a 250 mL quartz reactor.

LSV was obtained from the open-circuit potential (OCP) up to approximately 3.5 V at a scan rate of 50 mV s^{-1}. Light pulsed chronoamperometry was performed at 3 different potentials selected from the linear sweep voltammograms (1.8, 2.2 and 2.7 V). The light pulses were applied during 150 s, and the relaxation time (without the application of light) was also 150 s. EIS measurements were performed at the same DC potentials (E_{DC}) as those used for the chronoamperometric experiments. The amplitude of the AC component of the signal (E_{AC}) was 10 mV from peak to peak. Up to 50 frequency values from 1 kHz to 5 mHz separated logarithmically were tested.

To assess the effect of light on the electrochemical properties of the anode both LSV and EIS studies were performed in the presence and absence of a controlled light source. The light source was a Lightningcure LC8 L9566-03A (Hamamatsu) equipped with a 200 W Xenon lamp and an IR filter with a transmittance wavelength range from 350 to 600 nm.

2.4. Photoelectrochemical degradation of norfloxacin

The electrochemical and photoelectrochemical oxidation of the selected emerging pollutant was carried out using a synthetic solution of 100 mg L^{-1} of norfloxacin and 0.014 M Na_2SO_4 as supporting electrolyte. The working electrode was the Sb-doped SnO_2 anode coated with $BiPO_4$ with a total area of 25.8 cm^2. The same reactor as that employed in the electrochemical characterization was used, with an AISI 304 stainless-steel sheet counter electrode (with an area of 25.8 cm^2) and an Ag/AgCl reference electrode.

The degradation experiments were performed in galvanostatic mode at four current density values (7.75, 15.50, 23.25 and 31 mA cm^{-2}) in the absence and presence of light using the same light source as the one employed in the photoelectrochemical characterization experiments. The current was applied using a power supply (P1585, Peaktech). Samples were taken from the reactor every 15 min during the first hour, and then every 30 min. The effect of the illuminated area on the degradation was studied at 15.50 and 31 mA cm^{-2}. In this case, two values of illuminated area were compared: 5.7 cm^2 (single light beam) and 11.4 cm^2 (double light beam).

2.5. Analytical methods

The degradation of norfloxacin was followed using UV/vis spectrometry (Unicam UV4-200) by measuring the absorbance at 277 nm. The mineralization degree was evaluated through NPOC (Non-purgeable Organic Carbon) measurements (Shimadzu TNM-L ROHS). The anionic by-products were determined by ion chromatography (Metrohm 883 Basic IC). Norfloxacin intermediates formed during the degradation experiments were detected using high-performance liquid chromatography (HPLC) (Agilent 1290 Infinity) equipped with a C-18 column (Agilent ZORBAX Eclipse Plus). The method employed is described in previous works (Domingo-Torner et al., 2023). The concentration of persulfates present in solution was determined by means of iodometry as described in (Mora-Gómez et al., 2020).

3. Results and discussion

3.1. Physical characterization of the anode

The characterization of the ceramic matrix on which the photoactive layer was deposited was presented in previous works from the research group (Domingo-Torner et al., 2023), in which the porosity was estimated to be 50%. The color of the matrix is grey and has a slight blue tone which is characteristic of the dopant.

The synthesized photocatalyst was a whitish material, easy to grind. The three allotropes of $BiPO_4$ were identified in the X-ray diffractogram, where the two monoclinic phases were predominant, but a small proportion of the hexagonal phase was also detected (Fig. 1a). The reaction was considered complete since no phase reflections related to the raw materials were identified. The SEM analysis of the electrode surface showed that the catalyst was not homogeneously distributed over the substrate (Fig. 1b) as there were areas with higher accumulation of particles, and others quite clear, where the porous surface of the ceramic electrode can be seen. This heterogeneity in the distribution may be a consequence of the drying of the suspension. Particles that formed fluffy agglomerates after drying retained this characteristic, although sintering necks were visible between them. On the contrary, the particles that had formed more compact agglomerates after drying showed a higher level of sintering. The EDX analysis shown in Fig. 1c confirmed that the white particles were composed of P, Bi and O, but a signal from the tin oxide forming the electrode was also detected.

3.2. Photoelectrochemical characterization of the anode

The electrochemical characterization of the anode material began with the registration of the linear sweep voltammetric curves (LSV) in the absence and presence of light. These curves depict the dynamic response of the system in terms of current density.

The obtained LSV curves in the absence and presence of light, which are presented in Fig. 2a, exhibit three regions that can be attributed to

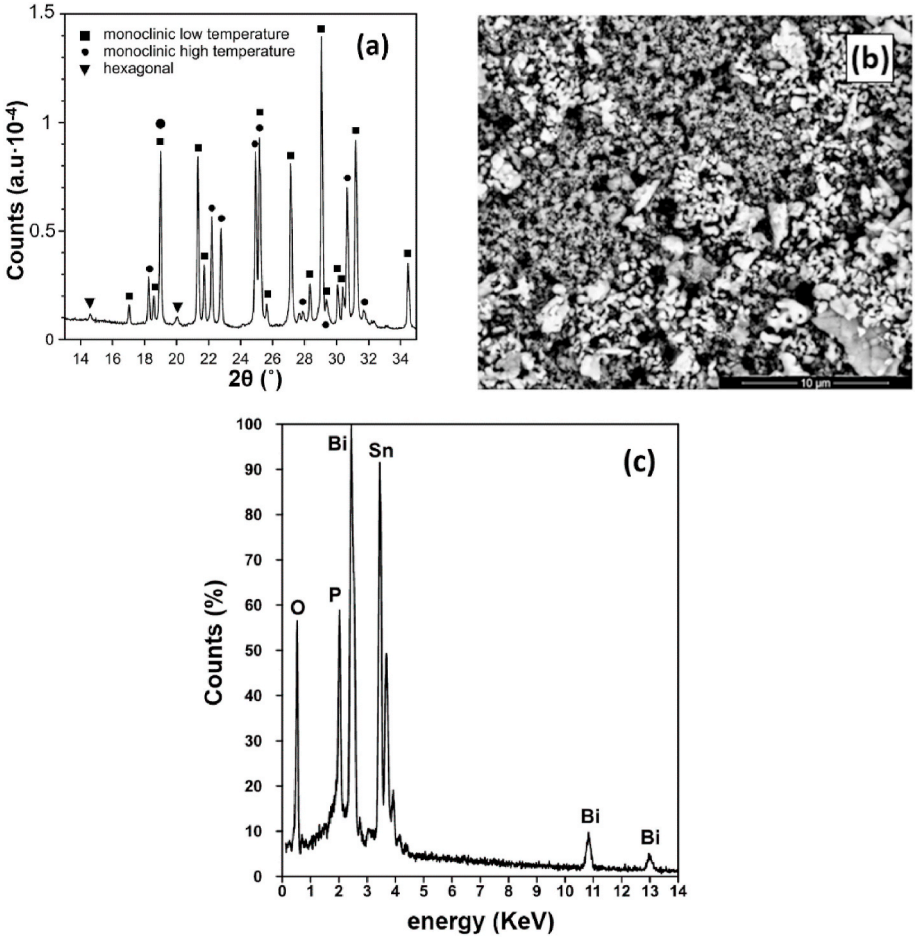

Fig. 1. Physical characterization of the anode (a) XRD (b) SEM (c) EDX.

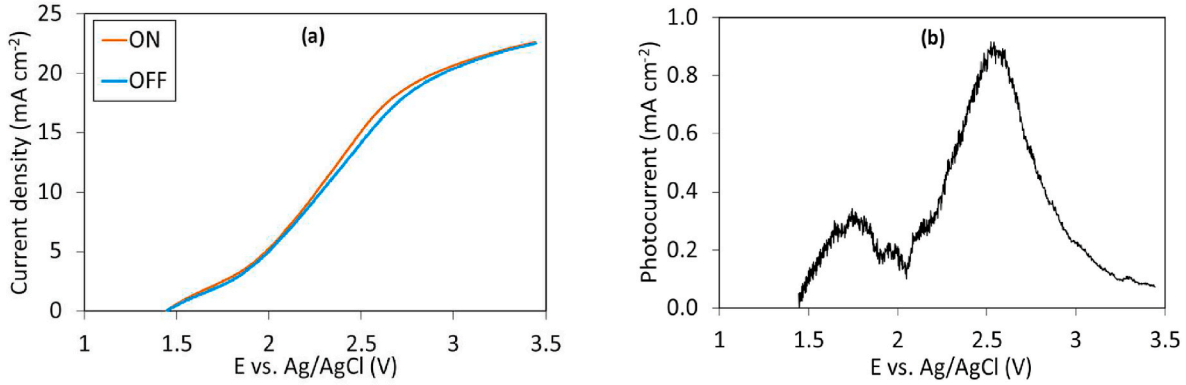

Fig. 2. (a) LSV curve obtained in the absence (OFF) and presence of light (ON). (b) Photocurrent response vs. potential.

different phenomena that take place on the anode. The first region presents a low slope that is associated with a high resistance to charge transfer. The fact that the ceramic matrix has a heterogeneous and microporous surface could explain this behavior since the anode surface does not charge homogeneously. The different phases of bismuth phosphate observed for the photoactive layer (see Fig. 1a), involve the presence of added surface heterogeneities and may contribute to an inhomogeneous activation of the anode surface at lower potentials.

Once all the surface is activated (at approximately 2 V), the curve shows a second region with an increased slope, and therefore, lower resistance. In this case, lower increments in potential are needed to increase the current. In this region, the complete electrode surface is evenly activated, and charge transfer phenomena take place efficiently. The saturation of the LSV is reached in the third zone, beyond which the slope decreases again. This could be attributed to the onset of the oxygen evolution reaction (OER) and the formation of bubbles that remain trapped in the electrode pores and block the contact between the electrolyte and the anode.

As it is also observed in Fig. 2, the anode exhibits higher current densities when illuminated, which corroborates the photoactivity of the $BiPO_4$ layer. However, the increment in the current density is low at potential values from 1.5 V to 2 V, which corresponds to the first zone of the voltammetric curve. The highest difference is observed at intermediate potential values (around 2.5 V). Therefore, it can be concluded that

the $BiPO_4$ layer also needs to be previously activated to show enhanced photoactivity. The evolution of the photocurrent with the applied potential is presented in Fig. 2b. The anode shows a low photocurrent response between 1.5 and 2 V, then reaches a maximum value at about 2.5 V, and decreases at higher potential values.

Three potential values were selected from Fig. 2a to perform the light-pulsed chronoamperometric experiments, which are shown in Fig. 3a. The anode showed instant response to light for all the applied potential values. However, at lower potential values, i.e., 1.8 V and 2.2 V, the photocurrent does not reach a stable value and increases steadily. On the contrary, at 2.7 V the photocurrent becomes stable almost immediately. At this potential value, the current response presents some noise owing to the formation of oxygen bubbles on the surface of the anode. The photocurrent response was higher at higher bias potentials, which agrees with the results observed in Fig. 2.

Electrochemical impedance spectra have been obtained at two potential values (1.8 V and 2.2 V) in the absence and in the presence of light. These values correspond to the first two zones of the LSV of Fig. 2a. The third zone was not studied because of the high instability of the system due to the generation of bubbles caused by the OER. The Nyquist diagrams for each of the conditions are presented in Fig. 3b. In general, all Nyquist plots exhibit a depressed semicircle, which is typical of systems with a nonideal behavior of the capacitive elements. This could be caused by the heterogeneity of the electrode surface, which stems from surface roughness, the presence of impurities, dislocations or grain boundaries (Growcock and Jasinski, 1989). The total resistance associated with the diameter of the semicircle, decreases with the potential, indicating that the semicircle is connected to OER kinetics. Moreover, the diameter of the semicircle decreases under the application of light, because of an improved charge transfer. The effect of light is more pronounced at a potential of 1.8 V, which agrees with the results shown in Fig. 2. The characteristic frequency corresponds to the frequency at which the maximum complex impedance (-Z'') is observed. This parameter is an indicator of the rate of the charge-transfer phenomena that occur on the surface of the anode. Charge-transfer processes become accelerated with an increase in the applied potential and with light, as denoted by higher values of characteristic frequency.

The preliminary electrochemical characterization of the electrode confirmed that the material has enhanced photoactivity at intermediate potential values (around 2.5 V, see Fig. 2), and therefore presents a lower charge transfer resistance. Moreover, the charge transfer resistance decreases in the presence of light (see Fig. 3b), corroborating the positive light effect on its electrochemical behavior.

3.3. Photoelectrochemical degradation of norfloxacin

As described previously, once characterized, the electrode has been applied to perform the electrochemical and photoelectrochemical degradation of norfloxacin at different values of applied current density and irradiated area. The evolution of the relative concentration of norfloxacin (C/C_0) with time for different irradiated areas and for the applied current values of 15.50 mA cm^{-2} and 31 mA cm^{-2} is presented in Fig. 4a and b, respectively. Two tendencies in the decrease of the relative concentration are observed, a linear decrease at the beginning of the experiment and an exponential one towards the end. Moreover, the degradation degree is higher for higher illuminated electrode areas. This is explained by the fact that the transport of electrons (thus, the formation of holes and its following reaction with water to form hydroxyl radicals) on the surface of the semiconductor is enhanced by light.

Regarding the kinetics of the process, the electrochemical degradation of most organic pollutants present in wastewater follows a mixed-order (pseudo-zero and pseudo-first order) kinetics, depending on the applied current density, electrolysis time, and concentration of the pollutant (Arenhart Heberle et al., 2019). Pseudo-zero order kinetics are attributed to processes without mass transfer limitation (high concentration of the pollutant) and with a slow generation of •OH. This behavior is mainly perceived at the beginning of the oxidation when the concentration of the pollutant in the bulk solution is high, whereas pseudo-first order kinetics are observed at the end of the experiment, where charge transfer limitations are not important (i.e., quick generation of •OH) but the concentration of the compound present in the bulk solution is low. In the present study, all experiments were fitted to a mixed-order kinetics model, since in all cases both tendencies previously described were observed. In the first stages, the generation of hydroxyl radicals is low and the concentration of norfloxacin is high. Towards the end of the experiment, the concentration of norfloxacin is low, which implies a mass transfer limitation of the molecule towards the anode.

The fitting of the experimental data to mixed-order kinetics is shown in Fig. 4 in the form of continuous lines. The two kinetic constants, k0 (pseudo-zero order) and k1 (pseudo-first order) were calculated and are represented against the applied current density in the absence (OFF) and presence of a double light beam (ON). The figures can be found in the supplementary information. The values of both k0 and k1 increase with the applied current density and the irradiated area (see Fig. S1), which confirms the existence of a synergistic effect between the electrogeneration and photogeneration of •OH.

The determination of the TOC values is important to quantify the degree of mineralization of norfloxacin because the degradation only shows how the norfloxacin molecule loses its primary structure. The mineralization degree serves to confirm that the norfloxacin molecule is indeed being eliminated and transformed into other smaller organic species and, ultimately, into CO_2 and H_2O. At low current densities (i.e., 15.50 mA cm^{-2}), the degree of mineralization of norfloxacin (TOC/TOC_0) is low in both photoelectrochemical and electrochemical experiments, and a slight effect of the presence of light is observed (see Fig. 5a). As the applied current density increases the relative TOC

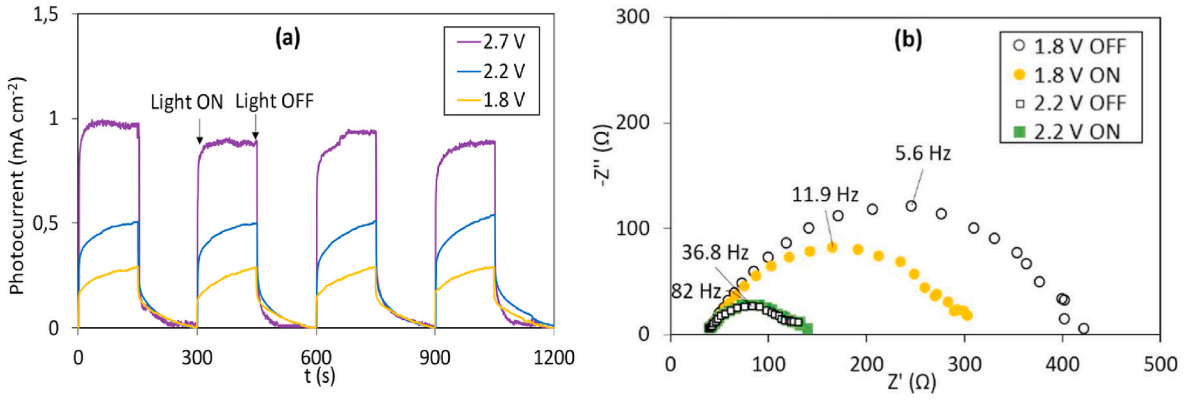

Fig. 3. (a) Light-pulsed chronoamperometry performed at 1.8, 2.2 and 2.7 V. (b) Nyquist diagram registered at 1.8 V and 2.2 V obtained in the absence (OFF) and presence of light (ON).

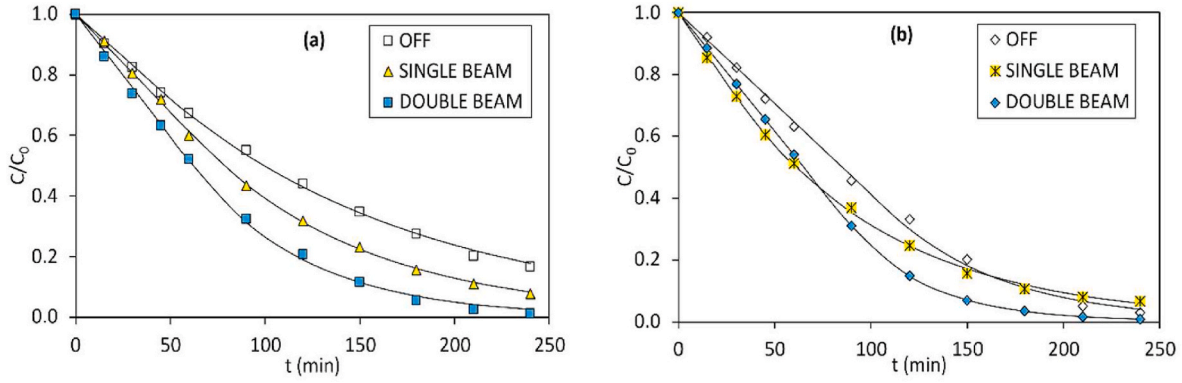

Fig. 4. Evolution of the relative norfloxacin concentration in the absence of light (OFF), with a single and double light beam at (a) 15.50 mA cm^{-2} and (b) 31 mA cm^{-2}. Fitting to mixed-order kinetics is presented in the form of continuous lines.

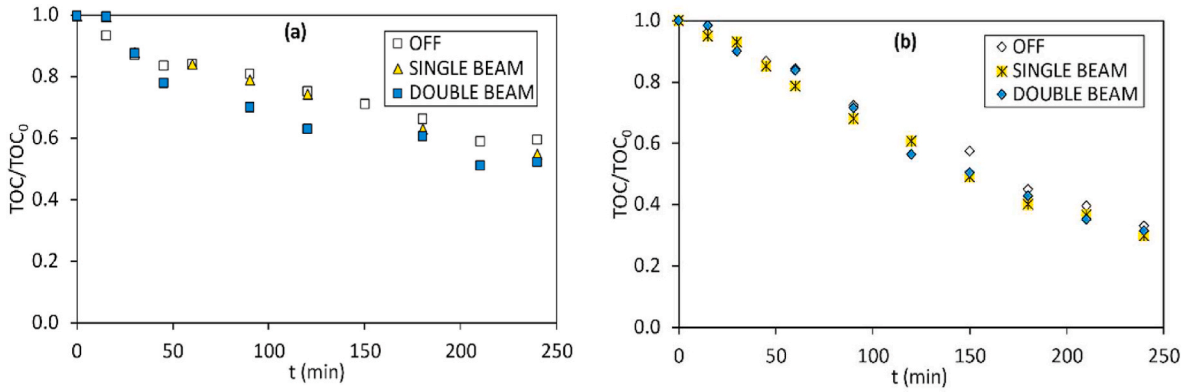

Fig. 5. Evolution of relative TOC concentration during electrochemical (OFF) and photoelectrochemical (ON) degradation experiments at (a) 15.50 mA cm^{-2} and (b) 31 mA cm^{-2}.

concentration becomes smaller and the effect of light is less significant (Fig. 5b). This behavior agrees with the results observed in the electrochemical characterization of the anode (see Fig. 2a), where the biggest effect of light is observed at intermediate current densities.

From the results presented in Figs. 4 and 5, it can be concluded that, generally, irradiating a larger area of the anode improves the degradation and the mineralization of the pollutant. Thus, from now on all the presented results will compare the electrochemical process with the photoelectrochemical one considering the largest illuminated area (double beam).

Ion chromatography was used to determine the concentration of low-molecular weight ions formed in the solution. The concentration evolution for fluoride and formate ions can be found in the supplementary material. Fluoride concentration increases with time with a similar trend at both current densities (see Fig. S2), and reaches a saturation value of about 5 mg L^{-1}. This concentration is very close to that resulting from the complete conversion of an initial concentration of norfloxacin of 100 mg L^{-1} according to Eq. (1): 5.9 mg L^{-1}. Comparing the data from Fig. 4 with the results of fluoride concentration observed in Fig. S2, it can be seen that beyond 150 min the amount of norfloxacin in the solution is very low, which coincides with the time at which the saturation in concentration of F^- ions is reached. Regarding the effect of light on fluoride generation, its concentration increases faster in the photoelectrochemical process, confirming a faster decomposition of norfloxacin.

$$C_{16}H_{18}FN_3O_3 + 29\,H_2O \rightarrow 16\,CO_2 + 3\,NH_4^+ + F^- + 64\,H^+ + 66\,e^- \quad (1)$$

Another ion detected by ion chromatography was formate ($HCOO^-$), whose concentration evolution is presented in the supplementary information at 15.50 mA cm^{-2} and 31 mA cm^{-2}, Fig. S3a and Fig. S3b, respectively. At 15.50 mA cm^{-2}, the $HCOO^-$ present in solution is higher in the photoelectrochemical experiments during the first 150 min. When light is applied, the concentration of formate increases faster and reaches a maximum at approximately 120 min. The concentration of $HCOO^-$ decreases after this maximum because of its subsequent mineralization at the latter stages of the experiment, where the rate of formate elimination is higher than its generation rate. At 31 mA cm^{-2}, the same phenomenon is observed both with and without illumination conditions; the larger generation of hydroxyl radicals at high current densities involves a faster destruction of formate ions.

Besides hydroxyl radicals, other oxidizing species could be generated in the electrochemical and photoelectrochemical processes. The sulfate ion present in the supporting electrolyte (Na_2SO_4) can oxidize to persulfate ($S_2O_8^{=}$), which is a highly oxidizing radical that can also take part in the degradation of norfloxacin (da Silva et al., 2019). However, previous norfloxacin ecotoxicological studies showed that persulfate ions are highly toxic (Montañés et al., 2020). The persulfate ion concentration formed at the end of each experiment is presented in the supplementary information and showed an increase in concentration with the applied current density (Fig. S4). However, the final persulfate concentration in solution is lower in the photoelectrochemical experiments, where approximately 50% less persulfates are generated. This could be explained by the fact that the light breaks the peroxide bond present in the persulfate ion (see Eq. (2)) to form two sulfate radicals (Piotr, 2019) which cannot be detected using the iodometry test. The sulfate radical is also used in the removal of organic pollutants because of its high oxidizing power (2.5–3.1 V) (Wang et al., 2022). Moreover, the sulfate radical has a higher half-life time (30–40 μs) than •OH (10^{-3} μs) (Wang

et al., 2021).

$$S_2O_8^{=} + h\upsilon \rightarrow 2\ SO_4^{\bullet -} \quad (2)$$

The intermediates formed during the degradation of norfloxacin were analyzed by HPLC-MS. Norfloxacin peak was detected at approximately 8 min and has an *m/z* value of 320.14. The formation and subsequent degradation of the intermediates of norfloxacin were followed by integrating the peak corresponding to each intermediate. The evolution of the area of two of the main intermediates is presented in Fig. 6 in the absence and presence of light. The proposed molecular structure for each of the intermediates is presented as inset in both figures.

In the case of the intermediate with a *m/z* value of 276.11 (Fig. 6a) at 15.50 mA cm^{-2} the peak area remains almost constant in the absence of light, meaning that the intermediate is not removed from the solution. In the photoelectrochemical degradation, its peak area reaches a maximum and then decreases, practically disappearing from the solution after 150 min. However, for an applied current density of 31 mA cm^{-2} the evolution of the peak area in the absence of light has the same behavior as that observed at 15.50 mA cm^{-2} in the photoelectrochemical degradation. The effect of light contributes to further oxidize the intermediate molecule, which is completely degraded from the minute 150 of the experiment. The evolution of the peak area of another intermediate with *m/z* 322.11 was also evaluated (Fig. 6b). A different tendency is observed for this compound. The effect of light is more relevant at 15.50 mA cm^{-2}, since a considerable higher peak area is obtained. This tendency is consistent with the degradation results, where at 15.50 mA cm^{-2} the difference between the electrochemical and photoelectrochemical degradation was more significant (see Fig. 4).

Both intermediates have a high organic content as can be seen in their molecular structure. According to the low mineralization degrees previously shown (Fig. 5), their complete removal from the solution after 150 min may indicate that they were degraded giving rise to smaller intermediates. Furthermore, as observed in Fig. 6, both identified intermediates contain a fluorine atom in its composition, and they are no longer detected from the minute 150 in almost all experiments (except at 15.50 mA cm^{-2} in the absence of light). These results help to justify the tendency observed in the fluoride ion concentration (Fig. S2), which remained constant from the minute 150. Beyond this time, there were no organic molecules with a fluorine atom present in solution, hence the concentration of fluoride ion remained constant until the end of the study.

3.4. Energy consumption

Two parameters associated with the energy consumption of the process were determined: the mineralization-specific energy consumption (E_{TOC}) and the mineralization current efficiency (MCE). The first parameter indicates which percentage of energy was invested in the mineralization of norfloxacin and was calculated using Eq. (3):

$$E_{TOC}\ \left(kWh\ kg_{TOC}^{-1}\right) = \frac{\int_0^t U_C(t)\cdot I(t)\ dt}{V\cdot\Delta[TOC]_t} \quad (3)$$

where U_C is the cell potential, I the applied current and V the volume of the reactor.

The increase in energy consumption is proportional to the applied current density (Fig. 7a). Lower specific energy consumption is observed in the presence of light since higher mineralization degrees are obtained in the photoelectrochemical process. The highest difference between the electrochemical and photoelectrochemical experiments is observed at 15.50 mA cm^{-2}, which is consistent with the data presented in Fig. 2. In the case of the highest applied current density, although the mineralization values obtained in the presence and absence of light are very similar, the light effect contributes to lower cell voltage values, and consequently, the energy consumption decreases.

The mineralization current efficiency determines how much of the applied current is used to mineralize the molecule of norfloxacin and can be calculated using Eq. (4) (Martí-Calatayud et al., 2022):

$$MCE\ (\%) = \frac{n\cdot F\cdot V\cdot(TOC_0 - TOC_t)}{7.2\cdot10^5\cdot m\cdot I\cdot t}\cdot 100 \quad (4)$$

where n is the number of electrons exchanged in the electrochemical oxidation assuming a complete mineralization of norfloxacin (66), see Eq. (1), F the Faraday's constant (96498 C mol^{-1}), TOC_0 -TOC_t is the difference in TOC values between the sampling time t and the initial value (mg L^{-1}), m is the number of carbon atoms present in norfloxacin (16) and $7.2\cdot10^5$ is a conversion factor (60 s $min^{-1}\cdot$12000 mg carbon mol^{-1}).

The decrease in mineralization current efficiency (Fig. 7b) with the applied current density is owed to the fact that the concentration of norfloxacin present in the solution is lower for higher current densities and the remaining molecules cannot diffuse properly towards the surface of the anode (Murugananthan et al., 2008). In the presence of light, the anode manifests higher mineralization current efficiencies. This tendency is reversed at 7.75 mA cm^{-2}, meaning that at this value of current density the number of oxidants generated photochemically is not significant. For 15.50 mA cm^{-2} and higher current densities, more oxidizing molecules are present in the solution because of their photoelectrochemical generation and the mineralization current efficiency is higher. The biggest difference is noted at the aforementioned current density, where the highest effect of light was also observed at both the degradation and the mineralization degrees, as mentioned previously.

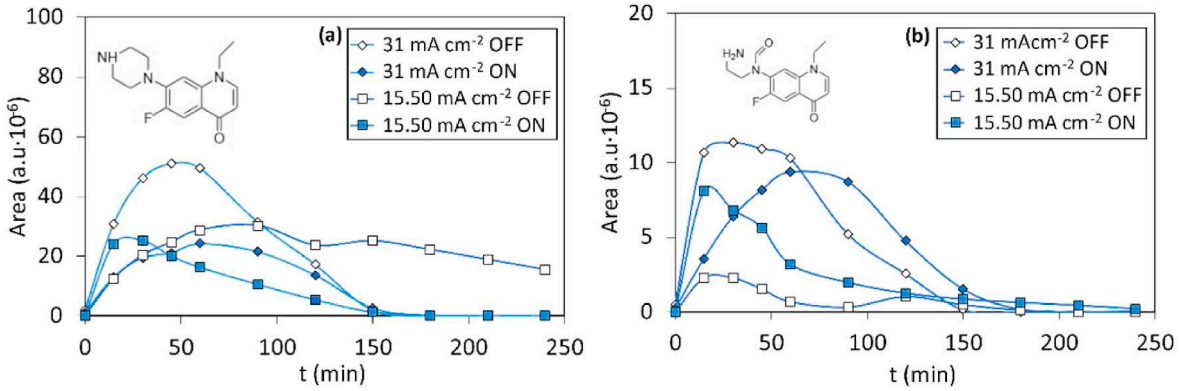

Fig. 6. Peak area evolution of the intermediates with (a) *m/z* = 276.11 and (b) *m/z* = 322.11 at 15.50 and 31 mA cm^{-2} in the electrochemical (OFF) and photoelectrochemical (ON) degradation experiments.

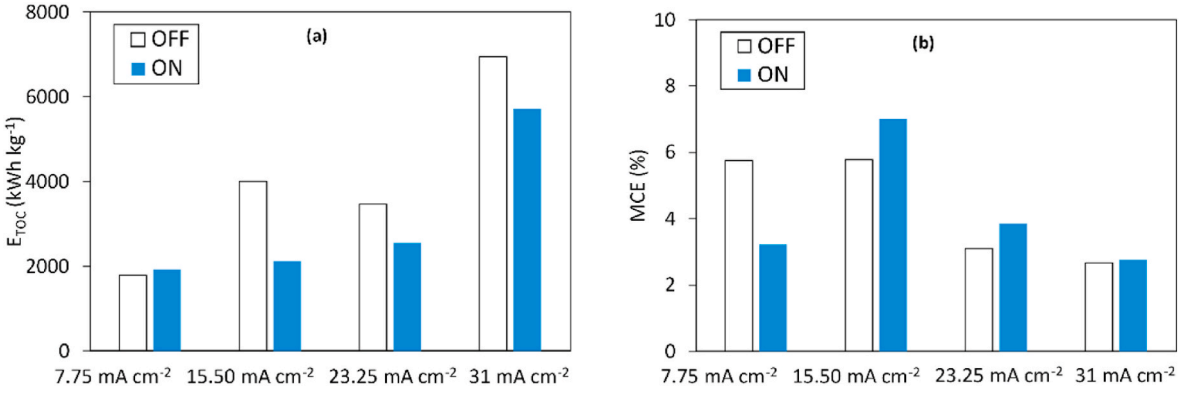

Fig. 7. (a) Average energy consumption and (b) average mineralization current efficiency in the electrochemical (OFF) and photoelectrochemical (ON) experiments.

4. Conclusions

In this study, the electrochemical response of a Sb-doped SnO_2 anode with a photocatalytic layer of $BiPO_4$ was evaluated. The anode exhibits higher current densities and a decreased charge transfer resistance in the presence of light and at intermediate applied potential values (approximately 2.5 V), where the heterogeneous electrode surface is evenly charged and the OER is still unimportant. Moreover, light-pulsed chronoamperometry confirmed the instantaneous anode response to light.

These results were confirmed in the electrochemical and photoelectrochemical degradation of norfloxacin experiments, where higher degradation degrees were obtained at intermediate current densities (15.50 mA cm^{-2}) and in the photoelectrochemical experiments. This was validated by the fact that higher degradation rates could be achieved when using larger illuminated areas (11.4 cm^2). The degradation of Norfloxacin followed a mixed-order kinetics. The higher values of kinetic coefficients obtained in the presence of light further corroborate the synergistic effect between the electrochemical and photochemical processes.

The evolution of by-product concentrations also confirmed the trends observed during the abatement of norfloxacin. Inorganic ions such as fluoride detached faster from the molecule in the photoelectrochemical experiments. Iodometry analysis proved the oxidation of the supporting electrolyte to persulfate ions, but their concentration decreased around 50% in the photoelectrochemical experiments, which may contribute to reduce the toxicity of the effluent significantly.

A positive effect of light was also observed in the energy consumption and the mineralization current efficiency parameters. At 15.50 mA cm^{-2} the mineralization-specific energy consumption decreased up to 53% in the presence of light as compared to the experiments in the absence of light. Current efficiency was also higher at lower current densities and in the presence of light.

Credit author statement

The first author Adele Balseviciute is responsible for the methodology and the development of the experimental section, Manuel Cesar Martí-Calatayud is responsible for writing the original draft of the paper, The corresponding author, Montse García-Gabaldón, is responsible for the supervision and the planification of the research activity, Sergio Mestre is responsible for the manufacture of the electrodes tested in this work, Valentín Pérez-Herranz is responsible for the Funding acquisition

Declaration of competing interest

The authors declare that they have no known competing financial interests or personal relationships that could have appeared to influence the work reported in this paper.

Data availability

The authors are unable or have chosen not to specify which data has been used.

Acknowledgements

The authors would like to express their gratitude to Conselleria d' Innovació, Universitats, Ciència i Societat Digital (Generalitat Valenciana, project reference: AICO/2021/128) for funding this research.

Appendix A. Supplementary data

Supplementary data to this article can be found online at https://doi.org/10.1016/j.chemosphere.2023.139173.

References

Arenhart Heberle, A.N., García-Gabaldón, M., Ortega, E.M., Bernardes, A.M., Pérez-Herranz, V., 2019. Study of the atenolol degradation using a Nb/BDD electrode in a filter-press reactor. Chemosphere 236, 124318. https://doi.org/10.1016/j.chemosphere.2019.07.049.

Bouddouch, A., Akhsassi, B., Amaterz, E., Bakiz, B., Taoufyq, A., Villain, S., Guinneton, F., el Aamrani, A., Gavarri, J.R., Benlhachemi, A., 2022. Photodegradation under UV light irradiation of various types and systems of organic pollutants in the presence of a performant $BiPO_4$ photocatalyst. Catalysts 12, 691. https://doi.org/10.3390/catal12070691.

da Silva, S.W., Navarro, E.M.O., Rodrigues, M.A.S., Bernardes, A.M., Pérez-Herranz, V., 2019. Using p-Si/BDD anode for the electrochemical oxidation of norfloxacin. J. Electroanal. Chem. 832, 112–120. https://doi.org/10.1016/j.jelechem.2018.10.049.

Domingo-Torner, C., García-Gabaldón, M., Martí-Calatayud, M.C., Mestre, S., Pérez-Herranz, V., 2023. Norfloxacin mineralization under light exposure using Sb–SnO_2 ceramic anodes coated with $BiFeO_3$ photocatalyst. Chemosphere 313, 137518. https://doi.org/10.1016/j.chemosphere.2022.137518.

Droguett, T., Mora-Gómez, J., García-Gabaldón, M., Ortega, E., Mestre, S., Cifuentes, G., Pérez-Herranz, V., 2020. Electrochemical Degradation of Reactive Black 5 using two-different reactor configuration. Sci. Rep. 10, 4482. https://doi.org/10.1038/s41598-020-61501-5.

El Rouby, W.M.A., Antuch, M., You, S.M., Beaunier, P., Millet, P., 2019. Novel nano-architectured water splitting photoanodes based on TiO_2-nanorod mats surface sensitized by ZIF-67 coatings. Int. J. Hydrogen Energy 44, 30949–30964. https://doi.org/10.1016/j.ijhydene.2019.08.220.

Fernández-Ibáñez, P., McMichael, S., Rioja Cabanillas, A., Alkharabsheh, S., Tolosana Moranchel, A., Byrne, J.A., 2021. New trends on photoelectrocatalysis (PEC): nanomaterials, wastewater treatment and hydrogen generation. Curr. Opin. Chem. Eng. 34, 100725 https://doi.org/10.1016/j.coche.2021.100725.

Goldstein, E.J.C., 1987. Norfloxacin, a fluoroquinolone antibacterial agent: classification, mechanism of action, and in vitro activity. Am. J. Med. 82, 3–17. https://doi.org/10.1016/0002-9343(87)90612-7.

Growcock, F., Jasinski, R.J., 1989. Time-resolved impedance spectroscopy of mild steel in concentrated hydrochloric acid. J. Electrochem. Soc. 136, 2310–2314. https://doi.org/10.1149/1.2097847.

Klein, E.Y., Van Boeckel, T.P., Martinez, E.M., Pant, S., Gandra, S., Levin, S.A., Goossens, H., Laxminarayan, R., 2018. Global increase and geographic convergence in antibiotic consumption between 2000 and 2015. Proc. Natl. Acad. Sci. USA 115, 3463–3470. https://doi.org/10.1073/pnas.1717295115.

Kumar, R., Raizada, P., Khan, A.A.P., Nguyen, V.H., van Le, Q., Ghotekar, S., Selvasembian, R., Gandhi, V., Singh, A., Singh, P., 2022. Recent progress in emerging

$BiPO_4$-based photocatalysts: synthesis, properties, modification strategies, and photocatalytic applications. J. Mater. Sci. Technol. 108, 208–225. https://doi.org/10.1016/j.jmst.2021.08.053.

Li, G., Ding, Y., Zhang, Y., Lu, Z., Sun, H., Chen, R., 2011. Microwave synthesis of $BiPO_4$ nanostructures and their morphology-dependent photocatalytic performances. J. Colloid Interface Sci. 363, 497–503. https://doi.org/10.1016/j.jcis.2011.07.090.

Martí-Calatayud, M.C., Dionís, E., Mestre, S., Pérez-Herranz, V., 2022. Antimony-doped tin dioxide ceramics used as standalone membrane electrodes in electrofiltration reactors enhance the oxidation of organic micropollutants. J. Clean. Prod. 363, 132342 https://doi.org/10.1016/j.jclepro.2022.132342.

Montañés, M.T., García-Gabaldón, M., Roca-Pérez, L., Giner-Sanz, J.J., Mora-Gómez, J., Pérez-Herranz, V., 2020. Analysis of norfloxacin ecotoxicity and the relation with its degradation by means of electrochemical oxidation using different anodes. Ecotoxicol. Environ. Saf. 188, 109923 https://doi.org/10.1016/j.ecoenv.2019.109923.

Mora-Gómez, J., García-Gabaldón, M., Carrillo-Abad, J., Montañés, M.T., Mestre, S., Pérez-Herranz, V., 2020. Influence of the reactor configuration and the supporting electrolyte concentration on the electrochemical oxidation of Atenolol using BDD and SnO_2 ceramic electrodes. Sep. Purif. Technol. 241, 116684 https://doi.org/10.1016/j.seppur.2020.116684.

Mora-Gómez, J., García-Gabaldón, M., Ortega, E., Sánchez-Rivera, M.J., Mestre, S., Pérez-Herranz, V., 2018. Evaluation of new ceramic electrodes based on Sb-doped SnO_2 for the removal of emerging compounds present in wastewater. Ceram. Int. 44, 2216–2222. https://doi.org/10.1016/J.Ceramint.2017.10.178.

Mora-Gómez, J., Ortega, E., Mestre, S., Pérez-Herranz, V., García-Gabaldón, M., 2019. Electrochemical degradation of norfloxacin using BDD and new Sb-doped SnO_2 ceramic anodes in an electrochemical reactor in the presence and absence of a cation-exchange membrane. Sep. Purif. Technol. 208, 68–75. https://doi.org/10.1016/j.seppur.2018.05.017.

Murugananthan, M., Yoshihara, S., Rakuma, T., Shirakashi, T., 2008. Mineralization of bisphenol A (BPA) by anodic oxidation with boron-doped diamond (BDD) electrode. J. Hazard Mater. 154, 213–220. https://doi.org/10.1016/j.jhazmat.2007.10.011.

O'Shea, K.E., Dionysiou, D.D., 2012. Advanced oxidation processes for water treatment. J. Phys. Chem. 3, 2112–2113. https://doi.org/10.1021/jz300929x.

Pan, C., Zhu, Y., 2010. New Type of $BiPO_4$ Oxy-acid salt photocatalyst with high photocatalytic activity on degradation of dye. Environ. Sci. Technol. 44, 5570–5574. https://doi.org/10.1021/es101223n.

Peleyeju, M.G., Umukoro, E.H., Tshwenya, L., Moutloali, R., Babalola, J.O., Arotiba, O. A., 2017. Photoelectrocatalytic water treatment systems: degradation, kinetics and intermediate products studies of sulfamethoxazole on a TiO_2–exfoliated graphite electrode. RSC Adv. 7, 40571–40580. https://doi.org/10.1039/c7ra07399b.

Piotr, Z., 2019. Decolorisation of methylene blue with sodium persulfate activated with visible light in the presence of glucose and sucrose. Water Air Soil Pollut. 230, 313. https://doi.org/10.1007/s11270-019-4372-x.

Polianciuc, S.I., Gurzău, A.E., Kiss, B., Georgia Ștefan, M., Loghin, F., 2020. Antibiotics in the environment: causes and consequences. Med. Pharm. Rep. 93, 231–240. https://doi.org/10.15386/mpr-1742.

Qian, R., Zong, H., Schneider, J., Zhou, G., Zhao, T., Li, Y., Yang, J., Bahnemann, D.W., Pan, J.H., 2019. Charge carrier trapping, recombination and transfer during TiO2 photocatalysis: an overview. Catal. Today 335, 78–90. https://doi.org/10.1016/j.cattod.2018.10.053.

Rayaroth, M.P., Aravind, U.K., Aravindakumar, C.T., 2016. Degradation of pharmaceuticals by ultrasound-based advanced oxidation process. Environ. Chem. Lett. 14, 259–260. https://doi.org/10.1007/s10311-016-0568-0.

Salimi, M., Esrafili, A., Gholami, M., Jonidi Jafari, A., Rezaei Kalantary, R., Farzadkia, M., Kermani, M., Sobhi, H.R., 2017. Contaminants of emerging concern: a review of new approach in AOP technologies. Environ. Monit. Assess. 189, 414. https://doi.org/10.1007/s10661-017-6097-x.

Seo, Y.S., Oh, S.G., 2019. Controlling the recombination of electron-hole pairs by changing the shape of ZnO nanorods via sol-gel method using water and their enhanced photocatalytic properties. Kor. J. Chem. Eng. 36, 2118–2124. https://doi.org/10.1007/s11814-019-0401-0.

Shokri, A., Mahanpoor, K., Soodbar, D., 2016. Evaluation of a modified TiO_2 (GO–B-TiO_2) photocatalyst for degradation of 4-nitrophenol in petrochemical wastewater by response surface methodology based on the central composite design. J. Environ. Chem. Eng. 4, 585–598. https://doi.org/10.1016/j.jece.2015.11.007.

Szymańska, U., Wiergowski, M., Sołtyszewski, I., Kuzemko, J., Wiergowska, G., Woźniak, M.K., 2019. Presence of antibiotics in the aquatic environment in Europe and their analytical monitoring: recent trends and perspectives. Microchem. J. 147, 729–740. https://doi.org/10.1016/j.microc.2019.04.003.

Tan, V.T., Vinh, L.T., 2020. Supported-metal oxide nanoparticles-potential photocatalysts. Photophysics, Photochemical and Substitution Reactions-Recent Advances. https://doi.org/10.5772/intechopen.93238.

UNESCO, 2014. Emerging Pollutants in Water and Wastewater. https://en.unesco.org/emergingpollutantsinwaterandwastewater.

Wang, J., Zheng, M., Deng, Y., Liu, M., Chen, Y., Gao, N., Du, E., Chu, W., Guo, H., 2022. Generality and diversity on the kinetics, toxicity and DFT studies of sulfate radical-induced transformation of BPA and its analogues. Water Res. 219, 118506 https://doi.org/10.1016/j.watres.2022.118506.

Wang, J., Zhuan, R., 2020. Degradation of antibiotics by advanced oxidation processes: an overview. Sci. Total Environ. 701, 135023 https://doi.org/10.1016/j.scitotenv.2019.135023.

Wang, W., Chen, M., Wang, D., Yan, M., Liu, Z., 2021. Different activation methods in sulfate radical-based oxidation for organic pollutants degradation: catalytic mechanism and toxicity assessment of degradation intermediates. Sci. Total Environ. 772, 145522 https://doi.org/10.1016/j.scitotenv.2021.145522.